Journal of Alloys and Compounds 509 (2011) 6321–6324

Contents lists available at ScienceDirect

Journal of Alloys and Compounds

journal homepage: www.elsevier.com/locate/jallcom

Structural, optical and magnetic properties of Eu-doped ZnO films

Yongsheng Tan[a,b], Zebo Fang[b], Wei Chen[b], Pimo He[a,*]

[a] Department of Physics, Zhejiang University, Hangzhou 310027, China
[b] Department of Physics, Shaoxing University, Shaoxing, 312000, China

ARTICLE INFO

Article history:
Received 20 September 2010
Received in revised form 11 March 2011
Accepted 15 March 2011
Available online 21 March 2011

Keywords:
Eu-doped ZnO films
Radio-frequency magnetron sputtering
Ferromagnetism
Magnetic measurements

ABSTRACT

Polycrystalline $Zn_{1-x}Eu_xO$ (x = 0, 0.02, 0.05) films were deposited on silicon (1 0 0) substrates by radio-frequency magnetron sputtering. The structural, optical and magnetic properties of the films were investigated. The results from both the X-ray diffraction and photoluminescence spectra reveal that Eu^{3+} ions successfully substitute for Zn^{2+} ions in the ZnO lattice. The magnetic field and temperature dependence of magnetization curves demonstrate that the $Zn_{0.95}Eu_{0.05}O$ films are ferromagnetic at room temperature. No impurity phase was found in Eu-doped films with X-ray diffraction, Raman spectroscopy and zero-field-cooled measurements. The ferromagnetism is attributed to the intrinsic property of Eu-doped ZnO films and could be interpreted by the bound-magnetic-polaron model.

1. Introduction

In the last few decades, diluted magnetic semiconductors (DMSs) have attracted enormous scientific interest because of their unique properties with both charge and spin degrees of freedom [1]. Much of work has been done on the magnetic properties of IV, III–V, and II–VI DMS materials obtained by doping magnetic impurities into those semiconductors [2,3]. Among them, ZnO-based DMSs have been extensively studied as they hold great potential for the applications in magneto-, photo-, spin-electronics and microwave devices due to their wide band gap (3.37 eV) and high exciton binding energy (60 meV) [4].

For the practical applications in magneto-, spin-electronic devices and so on, a DMS should be ferromagnetic above room temperature. Theoretical works predicted that transition metal (TM) doped ZnO would show ferromagnetic behavior above 300 K [5,6]. The ferromagnetism measured at various temperatures was reported in Co-, Ni-, Mn-, and Fe-doped ZnO [7–11]. Rare earth atoms have partially filled *f*-orbitals which carry magnetic moments and may take part in magnetic coupling as in the case of TMs with partially filled d-orbitals. Actually, recent experiments showed that rare earth metals such as Gd and Eu doped GaN exhibited ferromagnetic coupling [12–15]. On the other hand, rare-earth ions are good luminescence centers due to their narrow and intense emission lines originated from 4*f* intrashell transitions, and many investigations on the pure optical properties of Eu, Tb, and Er doped ZnO have been carried out [16–19]. Compared with TM doped ZnO, little attention has been paid to the ferromagnetic properties of rare earth metal doped ZnO. Therefore, it is of great importance to explore the magnetic properties of rare earth metal doped ZnO and promote its applications such as in magneto-optical and spin electronic devices.

In this paper, the structural, optical and magnetic properties of Eu-doped ZnO films prepared by radio-frequency (RF) magnetron sputtering were investigated and the origin of the ferromagnetism in the Eu-doped ZnO was also explored.

2. Experimental

The Eu-doped ZnO films with different Eu content ($Zn_{1-x}Eu_xO$ films, x = 0, 0.02 and 0.05) were deposited on silicon (1 0 0) substrates by RF magnetron sputtering. The ceramic targets of $Zn_{1-x}Eu_xO$ were synthesized from stoichiometric amounts of high purity ZnO (99.99% purity) and Eu_2O_3 (99.95% purity) powder. The pure argon (99.99% purity) or argon/oxygen premixed sputtering gas (oxygen content: 5%) were introduced to the chamber at a base pressure of 3×10^{-4} Pa. The substrate temperature, the working pressure and the deposition time were 450 °C, 1 Pa and 2 h, respectively. The structural properties of the samples were characterized by X-ray diffraction (XRD) in an error of about 1‰ and Raman spectroscopy. The surface morphologies of the thin films were investigated by scanning probe microscope (P47-SPM-MDT) in the atomic force microscope (AFM) mode. The room temperature photoluminescence (PL) spectra of the films were obtained with a Hitachi F-7000 fluorescence spectrophotometer. Magnetic properties were investigated by measuring magnetization as functions of magnetic field and temperature with a superconducting quantum interference device magnetometer (SQUID).

3. Results and discussion

Fig. 1 shows the XRD patterns of $Zn_{1-x}Eu_xO$ (x = 0, 0.02 and 0.05) films deposited on Si (1 0 0) with 5% oxygen content in the sputtering gas. The patterns indicate that all the films exhibit the *c*-axis

* Corresponding author. Tel.: +86 571 87953256; fax: +86 571 87951328.
E-mail address: phypmhe@dial.zju.edu.cn (P. He).

0925-8388/$ – see front matter © 2011 Elsevier B.V. All rights reserved.
doi:10.1016/j.jallcom.2011.03.084

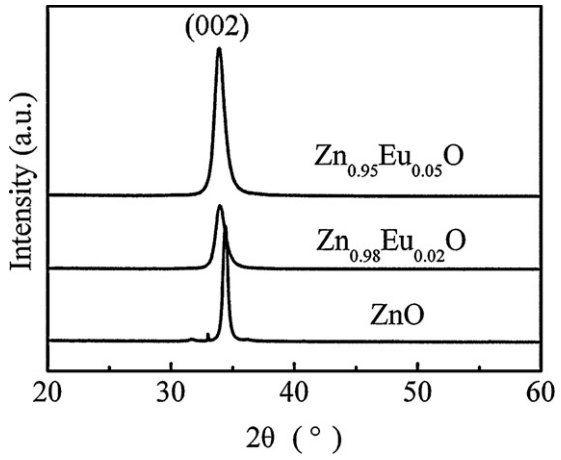

Fig. 1. XRD patterns of $Zn_{1-x}Eu_xO$ (x = 0, 0.02 and 0.05) films deposited with 5% oxygen content in the sputtering gas.

orientation without any impurity phases. The changes in the '*c*' lattice constants and the full widths at half maximum (FWHMs) of the (0 0 2) XRD peaks for $Zn_{1-x}Eu_xO$ films with increasing Eu concentration are summarized in Table 1 and the lattice constants determined with XRD at the present are in an error of about 1‰. Apparently, the '*c*' lattice constant increases from 5.214 Å to 5.282 Å with increasing Eu concentration from 0% to 5%. As the ionic radius of Eu^{3+} (1.07 Å) is much larger than that of Zn^{2+} (0.74 Å) [16], the increase of this '*c*' lattice constant indicates that Eu^{3+} ions successfully substitute for Zn^{2+} ions in the ZnO lattice. The FWHM of the (0 0 2) peak also increases from 0.459° to 0.935° with increasing Eu concentration from 0% to 5%. It could be attributed to a decrease in the grain size of the Eu-doped ZnO films. Fig. 2 shows the AFM images taken on the $Zn_{1-x}Eu_xO$ films. The decreasing of the grain size of $Zn_{1-x}Eu_xO$ films with increasing Eu concentration is clearly observed. The root mean square (RMS) roughness is 29.7, 6.26 and 3.42 nm for the films with Eu concentration of 0%, 2% and 5%, respectively.

Raman spectroscopy measurements were also performed to get more information about the microstructure of $Zn_{1-x}Eu_xO$ films. Fig. 3 shows the Raman spectra collected on $Zn_{1-x}Eu_xO$ (x = 0, 0.02 and 0.05) films with an excitation laser beam of He–Cd 325 nm. All the observed Raman peaks are nearly the same for the pure and Eu-doped ZnO films. The phonon mode at 578 cm^{-1} could be attributed to the E_1(LO) mode, which is caused by the defects such as O vacancy, Zn interstitial defect, or these complexes and free carriers [20]. The other three peaks are observed at 1156 cm^{-1}, 1735 cm^{-1} and 2312 cm^{-1} in turn, which are just the resonant bands of the E_1(LO) mode. These results indicate that there are large numbers of defects in our $Zn_{1-x}Eu_xO$ films. In addition, the presence of any other vibration mode from secondary phase is not observed in these Raman spectra.

Fig. 4(a) shows the room temperature PL spectrum of pure ZnO film with 320 nm excitation line of a xenon lamp. There are two emission bands on the spectrum. One is an intense and sharp emission band centered at about 387 nm, which is attributed to the near-band-edge (NBE) emission of ZnO. The other is a broad emission centered at about 554 nm, which is resulted from the ionized

Table 1
Changes in the '*c*' lattice constants and the FWHMs of the (0 0 2) XRD peaks for Eu-doped ZnO films with increasing Eu concentration.

Samples	'*c*' lattice constant	FWHM (°)
Pure ZnO	5.214	0.459
Zn0.98Eu0.02O	5.274	0.901
Zn0.95Eu0.05O	5.282	0.935

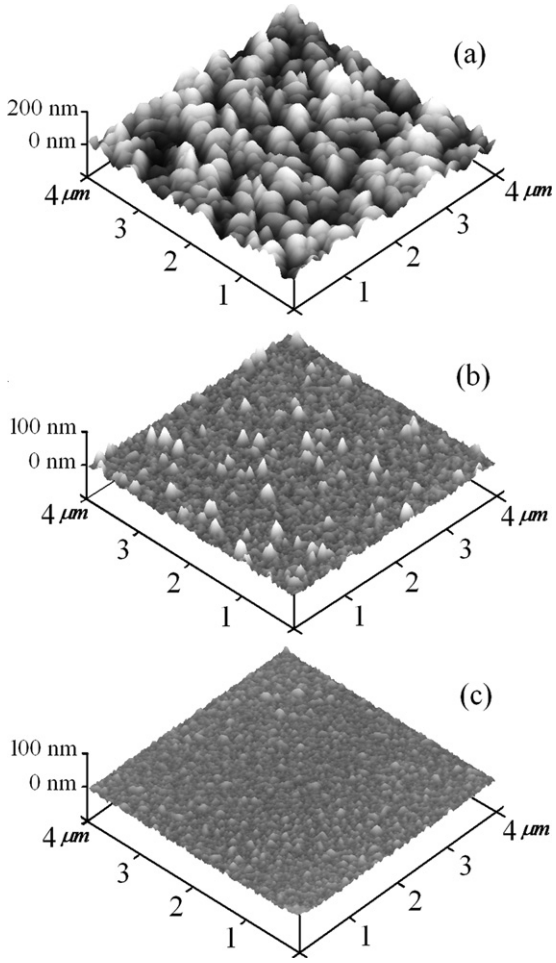

Fig. 2. AFM images of (a) pure ZnO, (b) $Zn_{0.98}Eu_{0.02}O$,and (c) $Zn_{0.95}Eu_{0.05}O$ thin films.

oxygen vacancies [10,21]. The presence of the 554 nm band indicates the existence of the defects, and is consisted with the Raman spectroscopy measurements, as discussed above. Fig. 4(b) shows the room temperature emission spectra of $Zn_{1-x}Eu_xO$ films under the excitation line of 468 nm. The peaks of red emissions at 595 nm and 618 nm are ascribed to the $^5D_0 \rightarrow {}^7F_1$ and $^5D_0 \rightarrow {}^7F_2$ transitions of Eu^{3+} ions, respectively [22]. The intensities of the red emissions increase with increasing Eu concentration, which indicates that Eu^{3+} ions substitute for Zn^{2+} ions in the lattice, and the efficient energy transfer from ZnO host to Eu^{3+} ions is achieved.

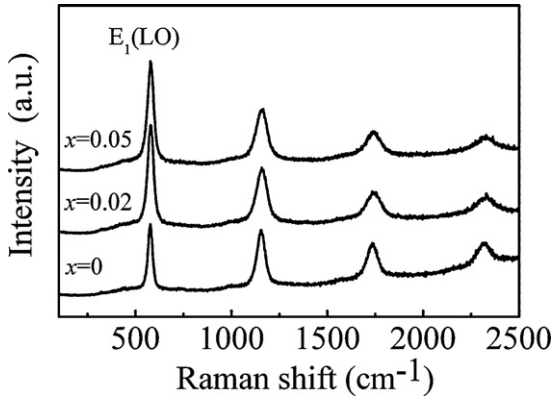

Fig. 3. Raman spectra of $Zn_{1-x}Eu_xO$ (x = 0, 0.02 and 0.05) films deposited on Si (1 0 0) substrates.

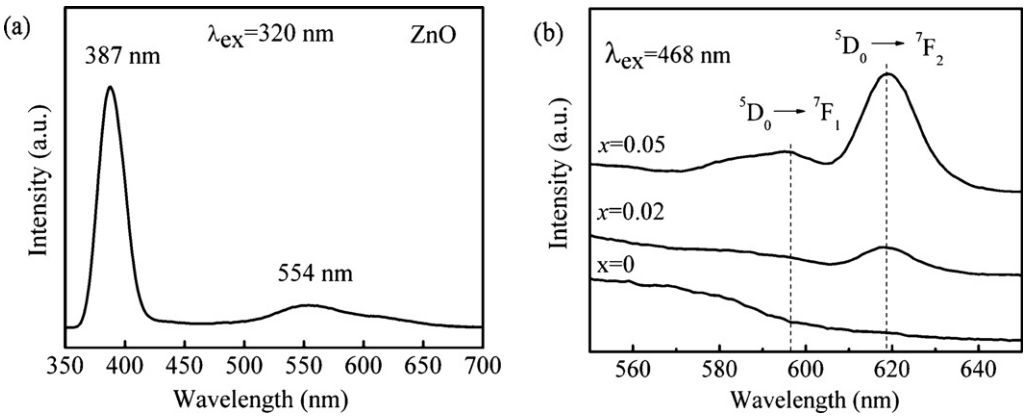

Fig. 4. (a) Room temperature PL spectrum of pure ZnO film with 320 nm excitation line of a xenon lamp, and (b) room temperature emission spectra of $Zn_{1-x}Eu_xO$ (x = 0, 0.02 and 0.05) films under the excitation line of 468 nm.

Fig. 5 exhibits the curves of magnetization versus applied field (M–H) for Eu-doped ZnO films. The inset is the zero-field-cooled (ZFC) curve of the $Zn_{0.95}Eu_{0.05}O$ film measured with a magnetic field of 200 Oe perpendicular to the sample surface. The pure ZnO shows linear diamagnetic signal even at low temperature [23]. Apparently, the $Zn_{0.98}Eu_{0.02}O$ film retains diamagnetic after subtracting the contribution of the substrate, which could be attributed to magnetic decoupling of Eu ions since the concentration of Eu is small (2%) in this sample. For the $Zn_{0.95}Eu_{0.05}O$ film, clear hysteresis loops are observed in the M–H curves both at 300 K and at low temperature down to 10 K, though the saturated magnetization is smaller for the M–H curve measured at 300 K. These results suggest that magnetic coupling occurs at a higher concentration of Eu (5%) for the Eu doped ZnO. Most importantly, these results show that room temperature ferromagnetism can be obtained by a proper quantity of Eu doping in ZnO film. For the ZFC measurement, the sample of $Zn_{0.95}Eu_{0.05}O$ was first cooled down to 10 K from room temperature under zero applied field, and then the net magnetization was measured with a magnetic field of 200 Oe during heating. The magnetization in the ZFC curve remains almost constant up to 300 K, indicating that the film is ferromagnetic and the Curie temperature of the film is higher than 300 K. It should also be noted that no discontinuous change in the ZFC curve confirms that the observed ferromagnetism can be attributed to the single magnetic phase without any phase-separation.

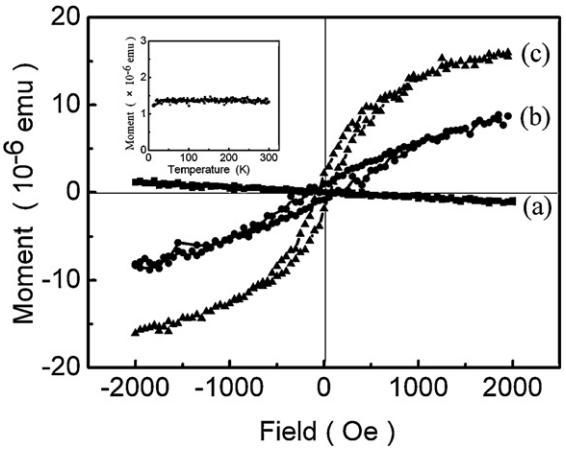

Fig. 5. M–H curves of (a) $Zn_{0.98}Eu_{0.02}O$ film, measured at 300 K, (b) $Zn_{0.95}Eu_{0.05}O$ film, measured at 300 K, and (c) $Zn_{0.95}Eu_{0.05}O$ film, measured at 10 K. The inset is the ZFC curve of the $Zn_{0.95}Eu_{0.05}O$ film measured with a magnetic field of 200 Oe perpendicular to the sample surface.

The ferromagnetism in $Zn_{0.95}Eu_{0.05}O$ film could arise from a number of possibilities, such as EuO, Eu metal, Eu_2O_3 and intrinsic property of the Eu-doped ZnO film. The existence of a secondary phase could be ruled out, since EuO is ferromagnetic with a T_C of 69 K [24], metallic Eu is helimagnetic with a Θ_N about 92 K, and Eu_2O_3 shows paramagnetic at 300 K. Furthermore, no impurity phase was found in Eu-doped ZnO films with XRD, Raman Spectroscopy and ZFC measurements. Therefore, ferromagnetism is expected to arise from the intrinsic exchange interaction of magnetic moments in $Zn_{0.95}Eu_{0.05}O$ film.

The exact mechanism of intrinsic ferromagnetism in ZnO-based DMSs is still under debate. In TM-doped ZnO systems, different mechanisms of ferromagnetism have been speculated. Hou et al. [25] reported that the carrier-induced ferromagnetism (RKKY mechanism) might be applied to explain the ferromagnetism in Cu-doped ZnO film. Meanwhile, Singhal et al. [26] reported that the bound-magnetic-polaron (BMP) is responsible for the ferromagnetism in Co-doped ZnO. Because the Raman and PL results showed that there were large numbers of defects in our $Zn_{1-x}Eu_xO$ films, the role of defects on the ferromagnetic properties was also studied. Fig. 6 shows the room temperature M–H curves of $Zn_{0.95}Eu_{0.05}O$ films deposited with different O_2 content. Although all the films show ferromagnetic at 300 K, but the saturated magnetization increases remarkably for the sample prepared in pure argon. Therefore, our results seem to be consistent with the BMP model proposed by Coey et al. [27]. The magnetic exchange interaction between O vacancy and Eu^{3+} ions aligns all the Eu^{3+} ions around the O vacancy, forming BMPs. Once the overlapping of BMPs crosses

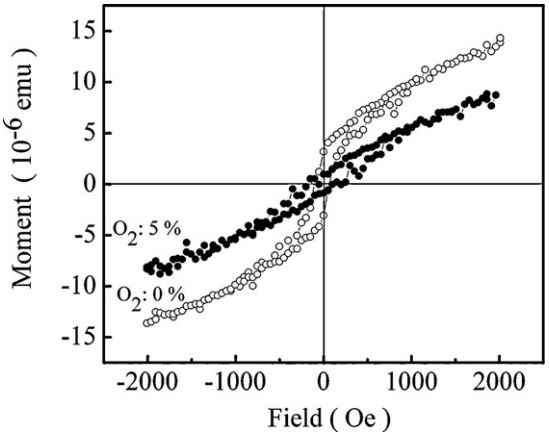

Fig. 6. Room temperature M–H curves of $Zn_{0.95}Eu_{0.05}O$ films deposited with different O_2 content.

over the sample, bulk ferromagnetism is created. More defects can be introduced due to the lack of oxygen when the film was sputtered with pure argon, which is responsible for the increase of the saturated magnetization for the sample prepared in pure argon.

4. Conclusions

Eu-doped ZnO films with a *c*-axis orientation have been grown on Si (1 0 0) substrates by RF magnetron sputtering. The structural and photoluminescence measurements reveal that Eu^{3+} ions substitute for Zn^{2+} ions in the lattice. Ferromagnetic loops were observed for $Zn_{0.95}Eu_{0.05}O$ films at 300 K, which demonstrated that room temperature ferromagnetism can be obtained from proper quantity of Eu doped ZnO films. No impurity phase was found in Eu-doped films with XRD, Raman spectroscopy and ZFC measurements. The ferromagnetism was attributed to the intrinsic property of Eu-doped ZnO films and could be interpreted by the bound-magnetic-polaron (BMP) model. More importantly, the present result, the ferromagnetism of Eu-doped ZnO above room temperature, also shows that Eu-doped ZnO can be practically used as a dilute magnetic semiconductor.

Acknowledgements

This work is supported by the Ministry of Science and Technology of China and the National Natural Science Foundation of China.

References

[1] H. Ohno, Science 281 (1998) 951.
[2] Y. Wang, F.X. Xiu, Y. Wang, X.F. Kou, A.P. Jacob, K.L. Wang, J. Zou, J. Alloys Compd. 508 (2010) 273–277.
[3] D. Soundararajan, P. Peranantham, D. Mangalaraj, D. Nataraj, L. Dorosinskii, J. Santoyo-Salazar, J.M. Ko, J. Alloys Compd. 509 (2011) 80–86.
[4] A. Kaushal, D. Kaur, J. Alloys Compd. 509 (2011) 200–205.
[5] T. Dietl, H. Ohno, F. Matsukura, J. Cubert, D. Ferrand, Science 287 (2000) 1019.
[6] T. Dietl, H. Ohno, F. Matsukura, Phys. Rev. B 63 (2001) 195205.
[7] A. Singhal, J. Alloys Compd. 507 (2010) 312–316.
[8] X.Y. Xu, C.B. Cao, J. Alloys Compd. 501 (2010) 265.
[9] Z. Yang, W.P. Beyermann, M.B. Katz, O.K. Ezekoye, Z. Zuo, Y. Pu, J. Shi, X.Q. Pan, J.L. Liu, J. Appl. Phys. 105 (2009) 053708.
[10] J. Lqbal, B.Q. Wang, X.F. Liu, D.P. Yu, B. He, R.H. Yu, New J. Phys. 11 (2009) 063009.
[11] C.Y. Lin, W.H. Wang, C.S. Lee, K.W. Sun, Y.W. Suen, Appl. Phys. Lett. 94 (2009) 151909.
[12] S. Dhar, O. Brandt, M. Ramsteiner, V.F. Sapega, K.H. Ploog, Phys. Rev. Lett. 94 (2005) 037305.
[13] J. Hite, G.T. Thaler, R. Khanna, C.R. Abemathy, S.J. Pearton, J.H. Park, A.J. Steckl, J.M. Zavada, Appl. Phys. Lett. 89 (2006) 132119.
[14] Y.K. Zhou, S.W. Choi, S. Kimura, S. Emura, S. Hasegawa, H.J. Asahi, Supercond, Nov. Magn. 20 (2007) 429.
[15] R. Wang, A.J. Steckl, N. Nepal, J.M. Zavada, J. Appl. Phys. 107 (2010) 013901.
[16] Y.Z. Zhang, Y.P. Liu, L.H. Wu, E.Q. Xie, J.T. Chen, J.Phys. D: Appl. Phys. 42 (2009) 085106.
[17] Y.H. Yang, Y. Feng, H.G. Zhu, G.W. Yang, J. Appl. Phys. 107 (2010) 053502.
[18] Z.B. Fang, Y.S. Tan, X.Q. Liu, Y.H. Yang, Y.Y. Yang, Chin. Phys. 13 (2004) 1330.
[19] X.Q. Gu, L.P. Zhu, Z.Z. Ye, H.P. He, Y.Z. Zhang, B.H. Zhao, Thin Solid Films 517 (2009) 5134.
[20] A.K. Pradhan, K. Zhang, G.B. Loutts, U.N. Roy, Y. Cui, A. Burger, J. Phys. Condens. Matter 16 (2004) 7123.
[21] Z.W. Liu, C.K. Ong, T. Yu, Z.X. Shen, Appl. Phys. Lett. 88 (2006) 053110.
[22] Y.P. Du, Y.W. Zhang, L.D. Sun, C.H. Yan, J. Phys. Chem. C 112 (2008) 12234.
[23] K. Potzger, S.Q. Zhou, F. Eichhorn, M. Helm, W. Skorupa, A. Mucklich, J. Fassbender, T. Herrmannsdorfer, A. Bianchi, J. Appl. Phys. 99 (2006) 063906.
[24] R.W. Ulbricht, A. Schmehl, T. Heeg, J. Schubert, D.G. Schlom, Appl. Phys. Lett. 93 (2008) 102105.
[25] D.L. Hou, X.J. Ye, X.Y. Zhao, H.J. Meng, H.J. Zhou, X.L. Li, C.M. Zhen, J. Appl. Phys. 102 (2007) 033905.
[26] R.K. Singhal, A. Samariya, Y.T. Xing, S. Kumar, S.N. Dolia, U.P. Deshpande, T. Shripathi, E.B. Saitovitch, J. Alloys Compd. 496 (2010) 324.
[27] J.M.D. Coey, M. Venkatesan, C.B. Fitzgerald, Nat. Mater. 4 (2005) 173.